Cell Research (2011) 21:922-933.
© 2010 IBCB, SIBS, CAS All rights reserved 1001-0602/10 $ 32.00
www.nature.com/cr

ORIGINAL ARTICLE

Aquaporin3 is a sperm water channel essential for postcopulatory sperm osmoadaptation and migration

Qi Chen[1, 2, *], Hongying Peng[1, *], Li Lei[1, 2, *], Ying Zhang[1, 2], Haibin Kuang[1, 2], Yujing Cao[1], Qi-xian Shi[3], Tonghui Ma[4], Enkui Duan[1]

[1]State Key Laboratory of Reproductive Biology, Institute of Zoology, Chinese Academy of Sciences, Beijing 100101, China; [2]Graduate School of Chinese Academy of Sciences, Beijing 100049, China; [3]Unit of Reproductive Physiology, Zhejiang Academy of Medical Sciences, Hangzhou 310013, China; [4]Central Research Laboratory, Bethune Second Hospital of Jilin University, 265 Ziqiang Street, Changchun 130041, China

In the journey from the male to female reproductive tract, mammalian sperm experience a natural osmotic decrease (e.g., in mouse, from ~415 mOsm in the cauda epididymis to ~310 mOsm in the uterine cavity). Sperm have evolved to utilize this hypotonic exposure for motility activation, meanwhile efficiently silence the negative impact of hypotonic cell swelling. Previous physiological and pharmacological studies have shown that ion channel-controlled water influx/efflux is actively involved in the process of sperm volume regulation; however, no specific sperm proteins have been found responsible for this rapid osmoadaptation. Here, we report that aquaporin3 (AQP3) is a sperm water channel in mice and humans. *Aqp3*-deficient sperm show normal motility activation in response to hypotonicity but display increased vulnerability to hypotonic cell swelling, characterized by increased tail bending after entering uterus. The sperm defect is a result of impaired sperm volume regulation and progressive cell swelling in response to physiological hypotonic stress during male-female reproductive tract transition. Time-lapse imaging revealed that the cell volume expansion begins at cytoplasmic droplet, forcing the tail to angulate and form a hairpin-like structure due to mechanical membrane stretch. The tail deformation hampered sperm migration into oviduct, resulting in impaired fertilization and reduced male fertility. These data suggest AQP3 as an essential membrane pathway for sperm regulatory volume decrease (RVD) that balances the "trade-off" between sperm motility and cell swelling upon physiological hypotonicity, thereby optimizing postcopulatory sperm behavior.

***Keywords*:** aquaporin3; sperm; osmoregulation; postcopulation

Cell Research (2011) **21**:922-933. doi:10.1038/cr.2010.169; published online 7 December 2010

Introduction

Studies in fish indicated that environmental osmotic changes trigger sperm motility [1, 2]. Interestingly, in most mammalian species examined, the sperm journey from the male to female reproductive tract also experiences a natural osmotic decrease [3, 4], implicating that an osmotic stress response upon ejaculation is evolutionarily conserved for normal sperm function. Indeed, increasing lines of evidence have shown that a physiological hypotonic stress could facilitate acrosome reaction in human sperm through calcium increase [5] and acrosome swelling [6], and is required for mouse sperm motility "start-up" once released from cauda epididymis [7], supporting the notion that a postcopulatory hypotonic stress is beneficial for normal sperm function. However, like a double-edged sword, the hypotonic stress could also cause potential harms to sperm function by inducing unwanted cell swelling [8, 9]. To counteract this negative impact, mammalian sperm have acquired mechanisms to drive rapid transmembrane water movement for efficient cell volume regulation [10]. Indeed, high water permeability has long been found in mammalian sperm [11-13], and ion channel-controlled water influx/efflux has been shown to be involved in postcopulatory sperm volume

*These three authors contributed equally to this work.
Correspondence: Enkui Duan
Tel: +86-10-64807182
E-mail: duane@ioz.ac.cn
Received 22 October 2010; revised 2 November 2010; accepted 3 November 2010; published online 7 December 2010

regulation [14-16]. However, the sperm protein(s) (such as plasma membrane channels) responsible for this trait have not been identified. Aquaporins (AQPs), a family of proteins that are believed to be involved in water transport [17], have been expected as potential candidates for sperm volume regulation due to their highly specialized function for water permeability [4, 10, 18]. Among the AQPs, AQP7 and 8 are expressed in rodent testis and sperm [19, 20], but genetic deletion of these AQPs in mice did not show obvious defects in the sperm function [21-23], possibly because of functional compensation by other AQP members. We previously identified that aquaporin3 (AQP3) is expressed in mouse testis [24], suggesting a potential role in male reproductive function. In this study, we demonstrated that AQP3 is a sperm water channel localized on the tail of mouse and human sperm. *Aqp3*-null sperm showed normal motility activation in response to hypotonicity, but with impaired volume regulation against hypotonic cell swelling, characterized by increased tail deformation due to excessive mechanical membrane stretch. Our data revealed that AQP3 functions as a key fluid regulator responsible for rapid sperm hypotonic osmoadaptation during the male-female reproductive tract transition, thus optimizing postcopulatory sperm behavior. Besides, the defect of the *Aqp3*-null sperm is clinically related, because similar sperm tail deformation is commonly found in clinical patients with male infertility/subfertility [25].

Results

AQP3 expression in sperm

AQP3 expression in mouse testis and sperm was detected at mRNA and protein levels (Supplementary information, Figure S1), which is in accordance with previous report that AQP3 is expressed in mouse testis [24]. We further found that AQP3 is specifically localized to the sperm tail during late spermatogenesis and sperm storage in epididymis (Figure 1A-1C). High-magnification immunofluorescence and immunogold electron microscopic analyses of isolated sperm from cauda epididymis further demonstrated that the localization of AQP3 was confined to the principal piece of the sperm tail membrane (Figure 1D-1G). In addition, immunofluorescence staining of AQP3 in ejaculated human sperm also showed highly specific expression at the principal piece of the sperm tail (Figure 1H), consistent with the localization detected in mouse sperm.

Aqp3$^{-/-}$ male shows impaired fertility

The prominent expression of AQP3 in the sperm led us to revisit the reproductive phenotype of *Aqp3*-null male. In the present study, each male mouse with different *Aqp3* genotypes was allowed to continuously mate with four wild-type females (each time with one female); after one successful mating (indicated by vaginal plug), the male was allowed to rest for 2 days before another female was placed in. The plugged females were individually caged and their pregnancy results were tracked. By this breeding assay, we found that although the *Aqp3*-null males could normally plug the females, the pregnancy rate and litter size were markedly lower compared with wild-type or heterozygous males. Nearly half of the wild-type females that mated with the *Aqp3*-null males showed no signs of pregnancy, and the remaining ones displayed reduced litter size (Table 1). These results clearly demonstrated that *Aqp3* deficiency resulted in impaired male fertility, strongly suggesting a crucial role of AQP3 in male reproduction.

Aqp3$^{-/-}$ males have normal sperm production and their sperm show normal motility activation in response to physiological hypotonicity

Initial examination of major male reproductive organs, including testis and epididymis, revealed no apparent differences between wild-type and *Aqp3$^{-/-}$* males in gross morphology and histology, as well as sperm count (Supplementary information, Figure S2A-S2C). As endocrine defects usually result in size and histological changes in reproductive organs, especially in seminal vesicles, these data suggest that endocrine defects are highly unlikely involved in the reduced fertility of *Aqp3*-null males, and the observed fertility decrease might be due to causes after sperm leave for female reproductive tract. Upon ejaculation, mouse sperm normally experience a physiological osmotic decrease from cauda epididymis (~415 mOsm) to uterine cavity (~310 mOsm) [26], which is beneficial for sperm motility activation. To determine the initial sperm motility activation between the wild-type and *Aqp3*-null sperm, we released cauda epididymal sperm directly into NaCl solution with different osmolarities and the sperm motility was assessed by Computer-Assisted Sperm Analyzer (CASA). As shown in Supplementary information, Figure S3A-S3E, both the genotypes of the sperm displayed lower-motility parameters in a relatively high osmolarity (440 mOsm) similar to the male reproductive tract, while in a relative hypotonic environment (300 mOsm) that mimics female uterine cavity, both showed robust motility activation.

Aqp3-deficient sperm undergo postcopulatory tail deformation due to increased vulnerability to hypotonic uterine environment

In contrast to the seemingly normal initial motility, the

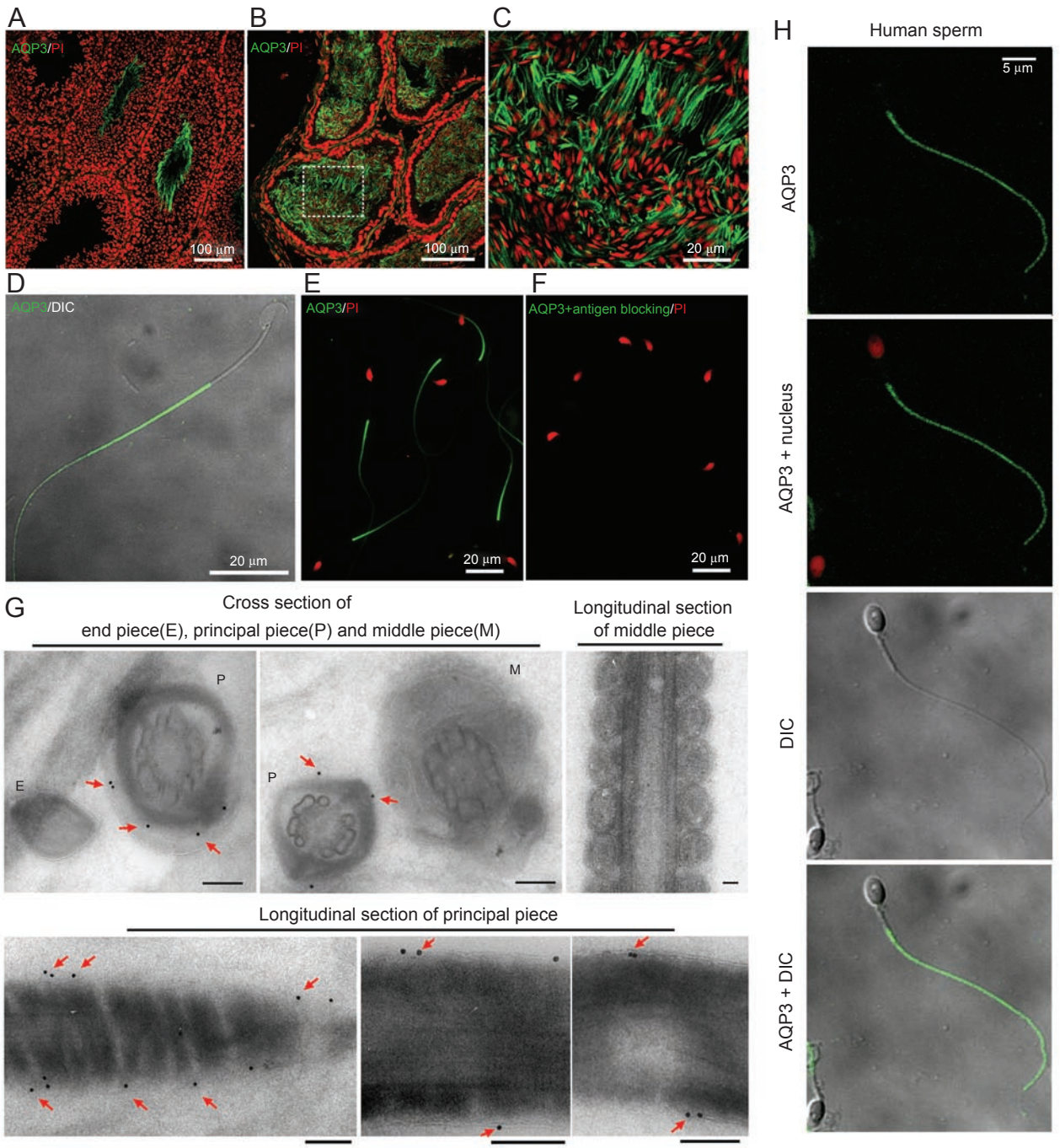

Figure 1 AQP3 is expressed in mouse sperm. **(A-D)** Immunofluorescence staining of AQP3 in mouse testis **(A)**, cauda epididymis **(B, C)** and isolated sperm **(D)** from cauda epididymis. Note the intensive green signal at principal piece of sperm tail. **(E, F)** AQP3 antibody staining in the absence **(E)** or presence **(F)** of competing immunogen. Nucleus was counter stained by propidium iodide (PI). **(G)** Immunogold-labeled electron microscopic detection shows that gold particles are stained at plasma membrane of the principal piece (indicated by arrows). Scale bars: 0.2 μm. **(H)** Immunofluorescence detection of AQP3 in human sperm.

Aqp3-null sperm showed increased tail deformation in the uterus after copulation (2 and 8 h), characterized by a typical appearance of hairpin-like bending (Figure 2A and 2B). The observed bending of the sperm is not likely

Table 1 Reproductive data of different *Aqp3* males mate with wild-type females

Genotype of mice		No. of male mice	No. of plugged females	Pregnancy rate	Average litter size
Male	Female			(No. of litter/mating)	(No. of pups/litter)
+/+	+/+	10	40	92.50% (37/40)	11.86±0.29 (439/37)
+/–	+/+	13	52	94.23% (49/52)	11.69±0.37 (573/49)
–/–	+/+	14	56	51.79%§§ (29/56)	8.59±0.90** (249/29)

Males (8 to 9 weeks old) with different *Aqp3* genotypes were used, each for sequential mating with four wild-type females. Successful mating was indicated by finding of vaginal plug. Pregnancy rate was calculated as the ratio of the number of females with pregnancy to the number of females with successful mating. When calculating average litter size, only the females that generated pups were included. The presented errors are shown in s.e.m. §§KO vs WT: $P = 0.0019$; KO vs Hetero: $P = 0.0004$, rank-sum test. **KO vs WT or Hetero: $P < 0.0001$, unpaired two-tailed *t*-test.

due to structural defects of flagellum as shown by electron microscopic analyses (Supplementary information, Figure S2D). *In situ* examination of the *Aqp3*-null sperm by immediate organ fixation also revealed no increased tail bending within cauda epididymis as compared with wild-type males (Figure 2A). These results indicate that the observed *in utero* sperm tail deformation is a post-copulatory defect that happens after the sperm enter the female reproductive tract.

The observed intrauterine tail bending in the *Aqp3*$^{-/-}$ sperm is markedly similar to previous reports that exposing normal sperm to drastic osmotic decreases (exposed to 150 mOsm PBS or distilled water) resulted in excessive cell swelling [7, 8]. Indeed, upon ejaculation, mouse sperm normally experienced a physiological osmotic decrease during the male-female reproductive tract transition (from ~415 to ~310 mOsm) [26], which is tolerable for most wild-type sperm to maintain normal morphology. Given that *Aqp3* deficiency results in the sperm tail bending after entering uterine environment, we hypothesized that the increased tail bending of the *Aqp3*$^{-/-}$ sperm could be due to abnormal drastic osmotic change upon ejaculation or intrinsic defects in response to physiological hypotonic stress.

By measuring the osmolarity of cauda epididymal fluid and uterine contents, we ruled out the first hypothesis, as the *in vivo* osmotic environments are comparable between wild-type and *Aqp3*-null mice (Figure 2C), which suggested that the abnormal tail bending of the *Aqp3*-null sperm is likely due to intrinsic defects, resulting in impaired resistance to hypotonic stress. To further define the impact of osmotic changes on the sperm tail bending, we performed an osmotic gradient challenge experiment on both the wild-type and *Aqp3*-null sperm. By directly releasing cauda epididymal sperm into different osmotic media (NaCl solution or HTF media), we found that at an osmolarity similar to cauda epididymis (440 mOsm), most sperm kept a straight form for both the genotypes. While at a lower osmolarity mimicking uterine environment (300 mOsm), the *Aqp3*-null sperm showed increased tail bending as compared with the wild-type sperm (Figure 2D and 2E). The wild-type sperm showed highly increased tail bending only at a much lower osmotic environment (150 mOsm) (Figure 2D and 2E).

Tail deformation in Aqp3$^{-/-}$ *sperm is caused by mechanical membrane stretch, followed by exaggerated cell swelling*

To confirm the hypothesis that the observed the sperm tail bending is caused by hypotonicity-induced cell swelling, the sperm volume changes were monitored using flow cytometric analyses, as reflected by the changing pattern in laser forward scatter (FSC), a sensitive method to simultaneously and objectively assess the sperm cell volume changes [27]. By comparing the pattern of FSC, it was shown that while both the wild-type and *Aqp3*-null sperm showed similar pattern at an osmolarity mimicking cauda epididymis (440 mOsm), the *Aqp3*-null sperm showed markedly increases in larger-size cell population in an osmotic environment mimicking uterine cavity (300 mOsm) (Figure 2F), indicating a sign of exaggerated cell swelling. These results clearly demonstrated that the sperm without AQP3 failed to control cell volume expansion under a physiological hypo-osmotic stress, which was responsible for the observed tail deformation.

By using time-lapse imaging recording, we further demonstrated the transforming process of how the abnormal cell expansion caused the sperm tail bending. As shown in Figure 3A and 3B, and Supplementary information, Movies S1 and S2, compared with the mild swelling of the wild-type sperm, the *Aqp3*-null sperm showed progressive volume expansion beginning at the site of cytoplasmic droplet (CD), then the increasingly expanded CD stretched the membrane, forcing the sperm tail to angulate and finally form a hairpin-like structure. In some swelling sperm cells, the membrane failed to stretch to such an extent and finally ruptured and the tail "straight out" (Figure 3C and Supplementary information, Movie S3). Scanning and transmission electronic microscopic image analyses further revealed that the

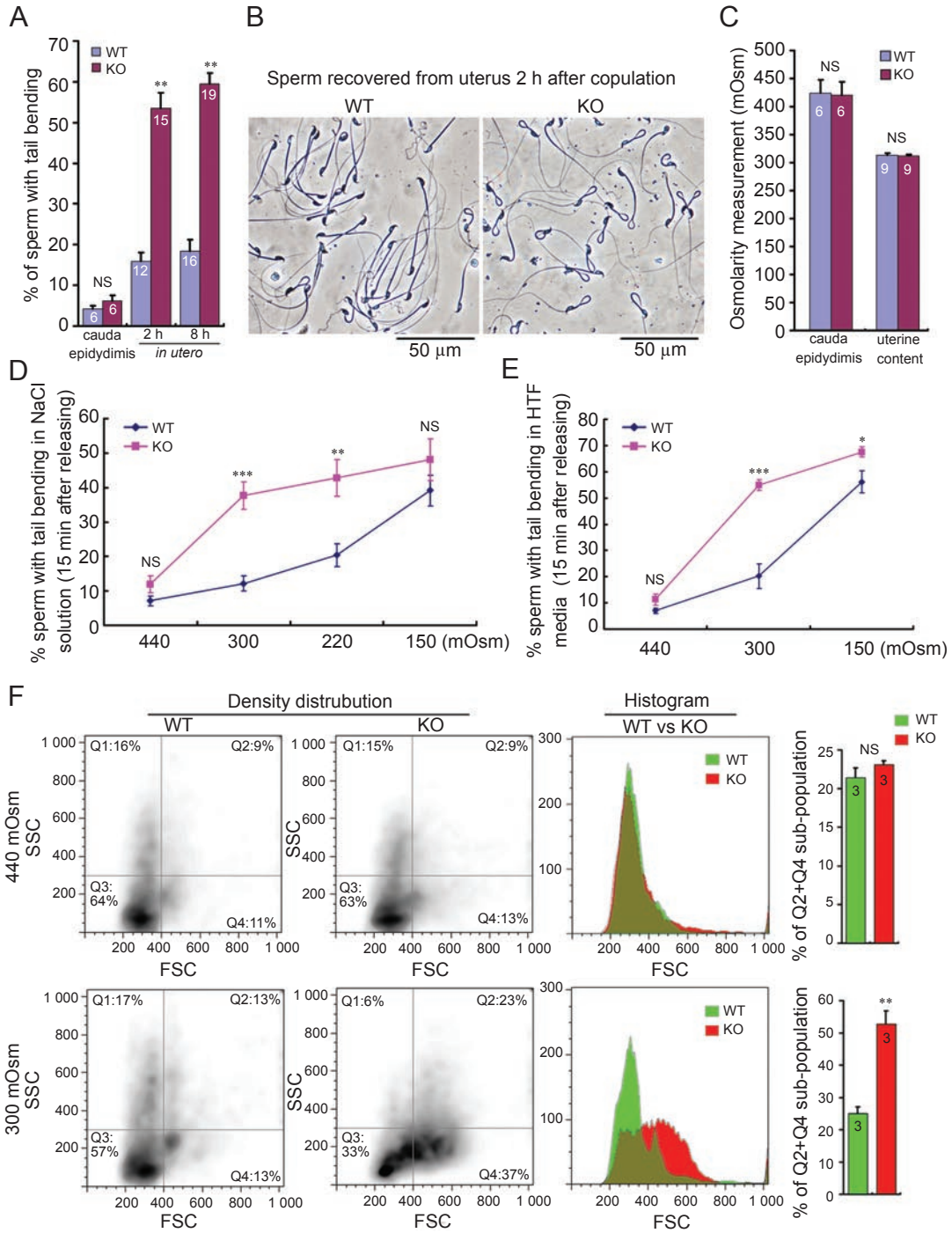

Figure 2 *Aqp3*$^{-/-}$ sperm showed increased *in utero* tail bending and exaggerated cell swelling upon physiological hypotonic stress. **(A)** Tail bending of wild-type and *Aqp3*$^{-/-}$ sperm in cauda epididymis and in postcopulatory uterus (NS: $P > 0.05$, $^{**}P < 0.0001$, *t*-test). **(B)** Demonstrative pictures of wild-type and *Aqp3*$^{-/-}$ sperm within uterus at 2 h after copulation. Scale bars: 50 μm. **(C)** *In vivo* osmotic environment of wild-type and *Aqp3*$^{-/-}$ sperm is comparable (NS: $P > 0.05$, *t*-test). **(D, E)** Examination of the sperm tail bending after releasing cauda epididymal sperm into different osmotic environment. NaCl solution ($n = 8$ for each data presented, NS: $P > 0.05$, $^{***}P < 0.0001$, $^{**}P < 0.005$. KO vs WT, *t*-test; **D**); HTF media ($n = 5$-8 for each data presented, NS: $P > 0.05$, $^{***}P < 0.0001$, $^{*}P < 0.05$. KO vs WT, *t*-test; **E**). **(F)** Flow cytometry recorded forward scatter laser (FSC) distribution of the wild-type and *Aqp3*$^{-/-}$ sperm within different osmolarities (NS: $P > 0.05$, $^{**}P < 0.005$, *t*-test). Numbers within the bars indicate number of mice used for each assay. All error bars represent s.e.m.

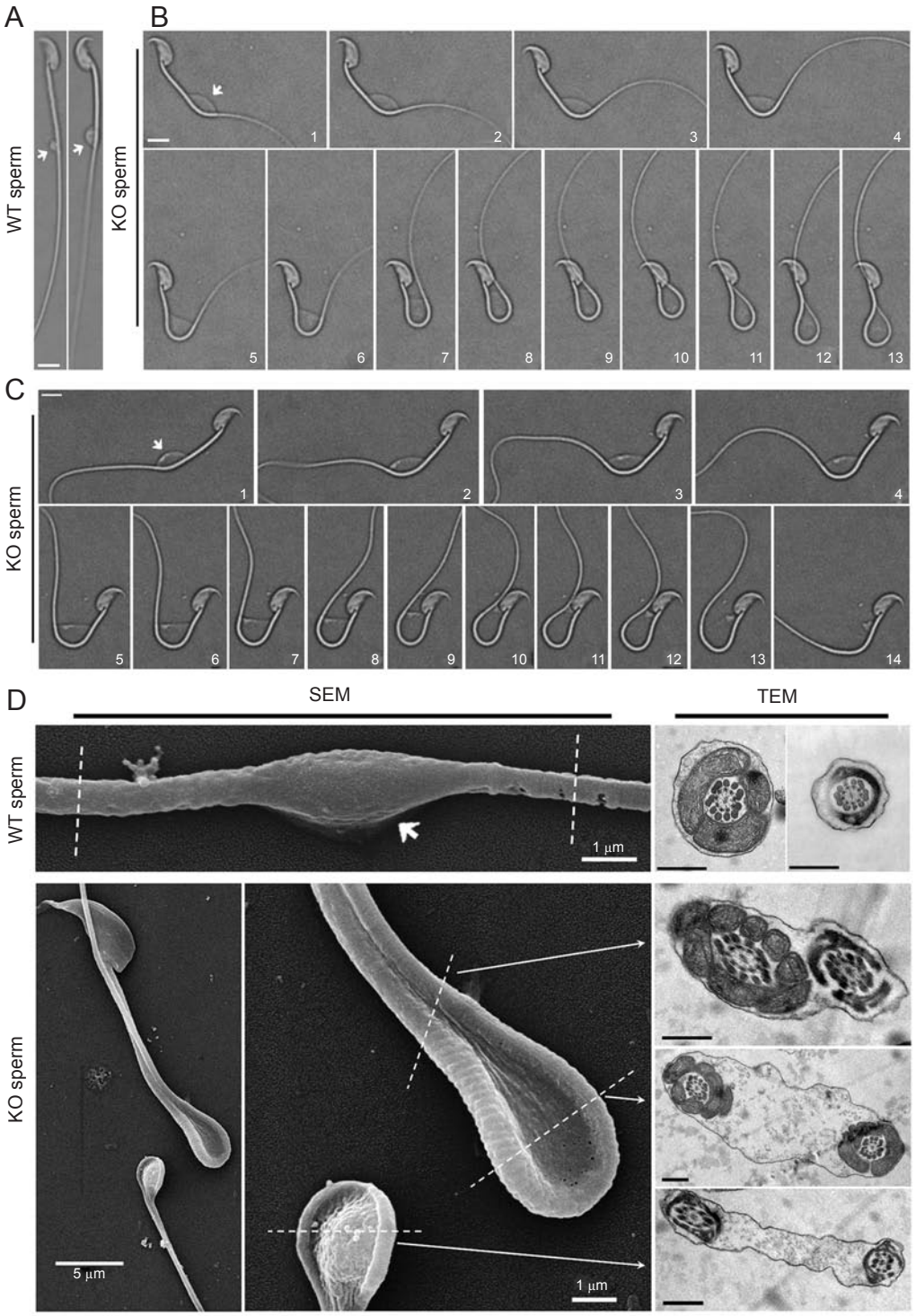

Figure 3 Sperm tail bending is caused by mechanical membrane stretch beginning at cytoplasmic droplet. **(A**-**C)** Images of wild-type **(A)** and *Aqp3*$^{-/-}$ **(B**, **C)** sperm from cauda epididymis that were directly released into 300 mOsm NaCl solution. For the *Aqp3*$^{-/-}$ sperm, time-lapse imaging reveals gradual process of sperm tail bending forced by membrane expansion. Numbers in the picture represent time sequential. Note the swelling state of cytoplasmic droplet (indicated by arrows) in each genotype. Membrane rupture could be clearly observed in 13th photo of **(C)**. Scale bars: 5 μm. **(D)** Scanning (SEM) and transmission (TEM) electronic microscopy reveal surface and inner appearance of sperm after releasing into 300 mOsm NaCl solution. Note: the bent *Aqp3*$^{-/-}$ sperm shows expanded intracellular space compared with the wild-type sperm. Scale bars (TEM): 0.5 μm.

hairpin portion of the bending sperm tail was encapsulated within the stretched membrane, forming a state with increased intracellular volume (Figure 3D). Due to the hypotonicity-induced tail deformation, although sperm from both genotypes showed similar initial motility parameters after epididymal release (Supplementary information, Figure S3A-S3E), a large number of *Aqp3*-null sperm showed low/no motility with tail bending 2 h after copulation (recovered from uterus) as compared with the wild-type sperm (Supplementary information, Movie S4 and S5), suggesting that the impaired sperm motility is a secondary effect following the sperm tail deformation.

Aqp3$^{-/-}$ sperm showed compromised in vivo fertilization due to impaired migration into oviduct

To examine the ability of the *Aqp3*-null sperm to fer-

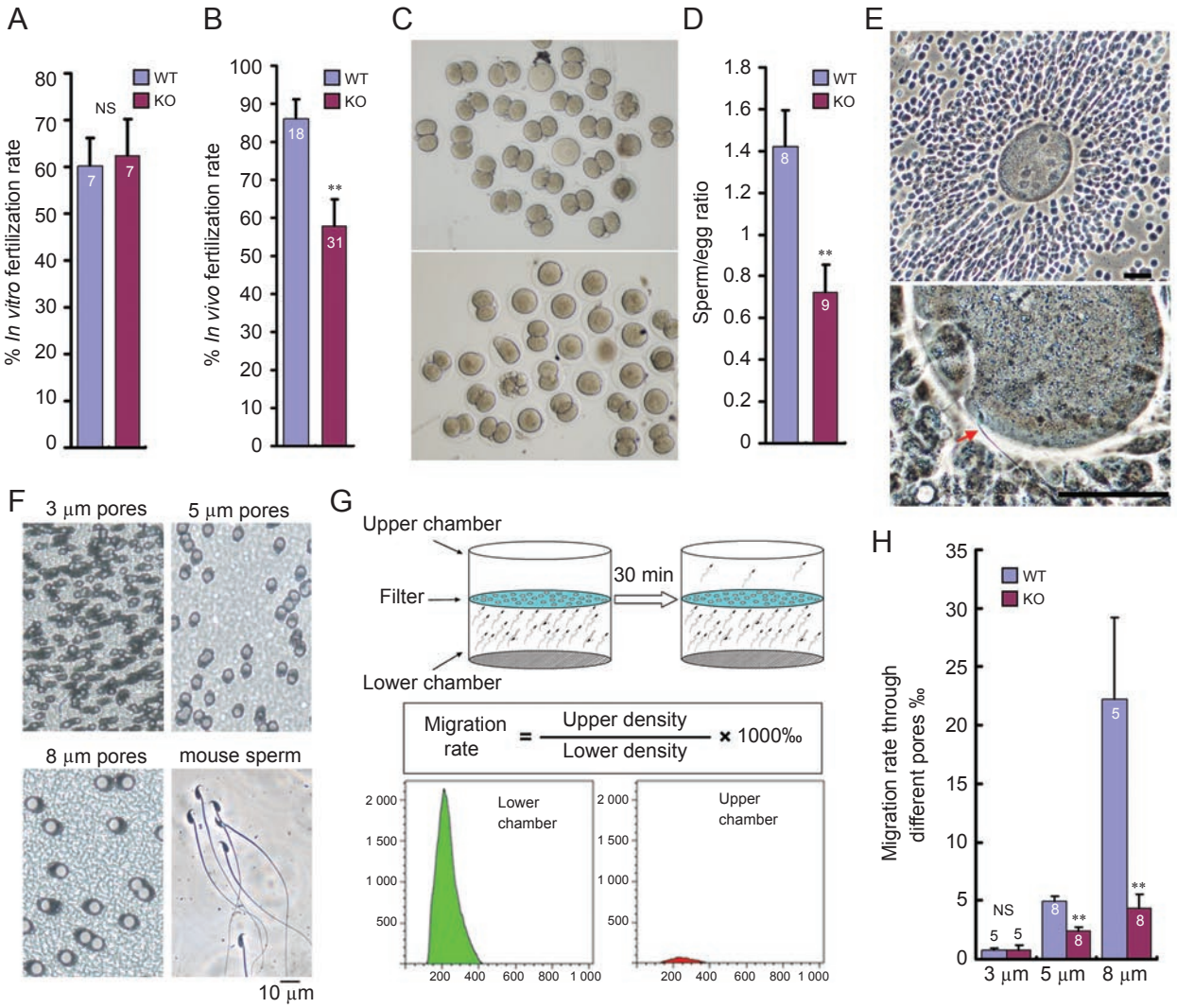

Figure 4 *Aqp3*$^{-/-}$ male shows reduced *in vivo* fertilization due to impaired sperm migration into oviduct. **(A**, **B)** *In vitro* **(A)** and *in vivo* **(B)** fertilization tests for wild-type and *Aqp3*$^{-/-}$ sperm (NS: $P > 0.05$, $^{**}P < 0.01$, *t*-test). **(C)** Representative pictures of embryos flushed from wild-type female oviduct (day 2) after mating with wild-type and *Aqp3*$^{-/-}$ male. Each picture shows embryos collected from two females. **(D)** *Aqp3*$^{-/-}$ sperm shows reduced number in reaching egg-cumulus complex *in vivo* ($^{**}P < 0.01$, *t*-test). **(E)** Demonstrative figures of egg-cumulus complex (upper) and arrived sperm as indicated by red arrow (lower). Scale bars: 50 μm. **(F)** Actual size of different pores (3, 5 and 8 μm diameter) in filter membranes (10 μm thick) used for *in vitro* sperm migration assay. **(G)** Illustration of *in vitro* sperm migration assay through filters with different pores and calculation of migration rate. **(H)** Migration rate for wild-type and *Aqp3*$^{-/-}$ sperm (released from cauda epididymis) through different filters (NS: $P > 0.05$, $^{**}P < 0.01$, KO vs WT, *t*-test). Numbers within or above the bars indicate number of mice used for each assay. All error bars represent s.e.m.

tilize eggs, we performed *in vitro* and *in vivo* fertilization tests in wild-type and *Aqp3*$^{-/-}$ males. Interestingly, under a standard protocol of *in vitro* fertilization, sperm of both the genotypes showed similar ability in fertilizing wild-type eggs (Figure 4A). However, *in vivo* fertilization test revealed a significant decrease in fertilization rate in the *Aqp3*$^{-/-}$ male (Figure 4B and 4C). The discrepancy between *in vitro* and *in vivo* fertilization rates led to the conclusion that the *Aqp3*-null sperm showed no intrinsic problem in fertilization once they could reach the eggs in culture media, while the decreased *in vivo* fertilization rate might be due to decreased number of sperm reaching the eggs in the oviduct. Under physiological condition, before reaching the eggs, sperm must successfully migrate through the uterine-oviduct junction, where most of the sperm were blocked out and stayed in the uterine cavity. By checking the number of sperm that arrived in the egg/cumulus complex after time-defined copulation [28], we found a significant decrease in sperm/egg ratio in the *Aqp3*-null male (Figure 4D and 4E), supporting the idea that the impaired *in vivo* fertilization in the *Aqp3*$^{-/-}$ male is due to reduced sperm number that migrated to oviduct. Moreover, *in vitro* sperm transwell migration assay demonstrated that the *Aqp3*-null sperm showed decreased ability in passing through the mesh pores of membrane filter that mimicked the barrier of uterine-oviduct junction (Figure 4F-4H and Supplementary information, Figure S4), which further justified our hypothesis. The scenario of AQP3 on sperm osmoregulation and migration was illustrated in Figure 5.

Discussion

In summary, our data provided direct evidence suggesting that AQP3 is a key fluid regulator essential for sperm regulatory volume decrease (RVD) upon hypoto-

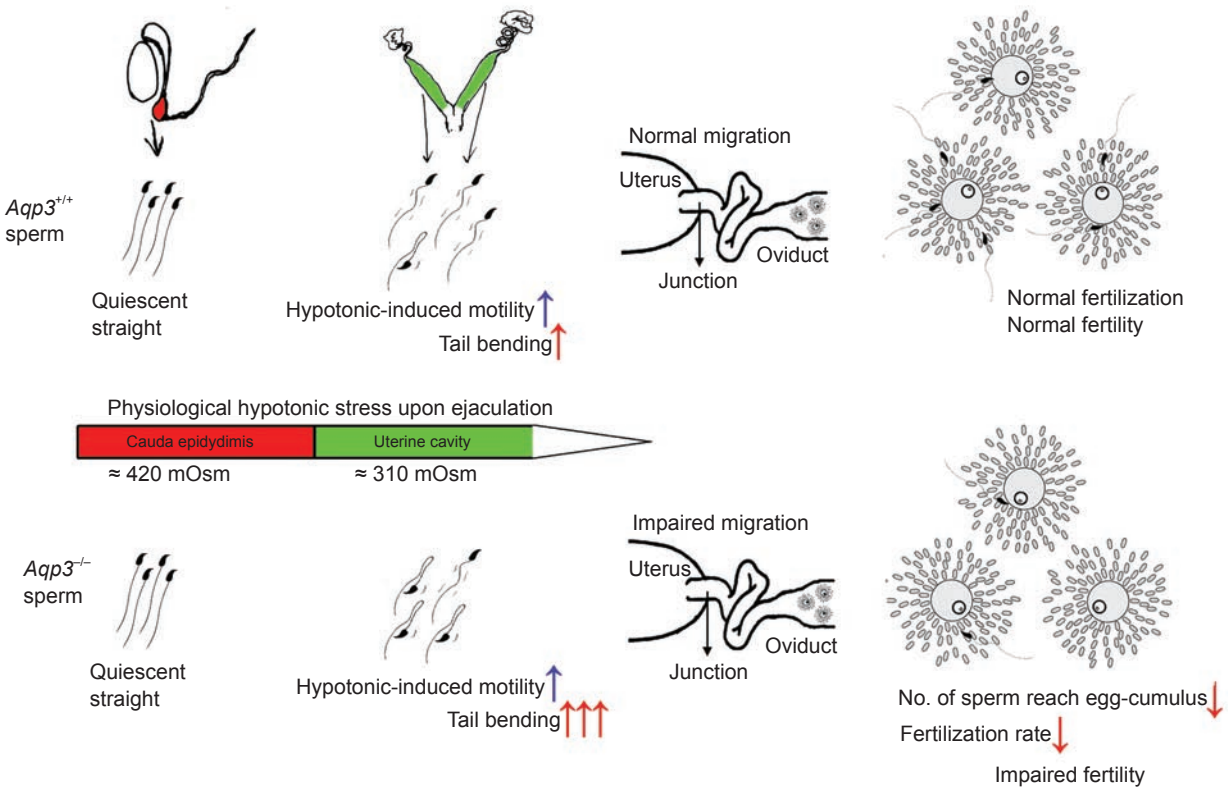

Figure 5 Schematic figure summarizing the scenario of how AQP3 deficiency impairs male fertility. Upon ejaculation, sperm stored in male reproductive tract enter uterine cavity where they experience a natural osmotic decrease. The physiological hypotonic stress initiates sperm motility, but also poses potential harms to sperm function by inducing sperm cell swelling. Normally, only a small portion of sperm undergoes tail deformation because of the hypotonic stress. However, in *Aqp3*$^{-/-}$ mice, the *Aqp3*$^{-/-}$ sperm showed impaired resistance and increased vulnerability to hypotonic-induced cell swelling, resulting in a large portion of sperm showing tail bending after entering uterine environment. The increased tail deformation in the *Aqp3*$^{-/-}$ sperm led to decreased sperm passage through uterine-oviduct junction and decreased chance for meeting and fertilizing eggs, resulting in impaired male fertility.

nicity-induced cell swelling. It was revealed that while sperm utilize postcopulatory hypotonicity for motility activation, AQP3 serves to protect sperm from swelling-induced mechanical membrane stretch, thus optimizing the "trade-off" between sperm motility and cell swelling upon physiological hypotonicity. To our knowledge, this is the first identified sperm protein responsible for efficient postcopulatory sperm osmoadaptation, thereby influencing male fertility. However, the *Aqp3*$^{-/-}$ male is not completely infertile, suggesting that the physiological events of sperm cell regulation should involve other members of AQP family or other membrane channels with compensatory functions. Indeed, RVD process involves active ion influx/efflux of various kinds [29], and many of these ion fluxes have been shown present in sperm. Therefore, further identifying specific ion channels in sperm will be undoubtedly important for a deeper understanding of sperm physiology, especially during the process of postcopulation.

The exact mechanisms by which AQP3 regulates sperm water outlet and the involvement of RVD are still not clear, one possibility is that the spatial arrangement of multiple AQPs (AQP3, 7 and 8) along the specialized architecture of the sperm tail would provide optimal sperm function, the previously found AQP7 and 8 in sperm might serve as major water influx, while AQP3 as the major efflux pathway. Also, it is more likely that AQP3 might serve as a part of the osmosensing system responsible for detecting early events in cell swelling (as a mechanosensor) and conveying signal to the subsequent RVD process, as firstly revealed by mathematical models [30]. Indeed, recent years have witnessed growing evidence supporting a critical role of AQPs (AQP1, 2, 3 and 5) during RVD process in various cell systems [31-34], suggesting that AQPs might have alternative regulatory functions in membrane fluid transport, not just inert pores simply increasing the osmotic permeabilities. As AQP3 is an aquaglyceroporin with permeability to both water and glycerol [17], there is also an open but intriguing possibility that AQP3 might have unique plastic molecular structure that responds to changing cell environment, or AQP3 could facilitate glycerol transport in sperm cell as a potential energy substrate, which is an interesting issue that warrants further investigation. More radically, given the recent contention that an ion pump or channel is evolutionally changeable or even coexisted in one molecule with hybrid behavior [35] and the most recent unexpected finding that the formate transporter shows an AQP-like channel structure [36, 37], it is encouraging to propose that an AQP might have the potential to function as an active water transporter (combined with other molecules) during processes such as sperm osmoregulation. Nonetheless, previous reports, coupled with present data on AQP3-mediated sperm cell volume regulation, would provide future directions for a new round of AQP research toward more fundamental roles as general regulators of living cells, possibly with unexpected novel mechanisms.

Another interesting issue in this study is about the functional observation of the sperm CD, for mammalian sperm, the physiological functions of the CD remain enigmatic [38], although its structure is clear and it has been successfully utilized for sperm cell patch claming in analyzing sperm membrane ion flow [39, 40]. Our data clearly showed that when sperm face physiological hypotonic stress (from ~420 to ~300 mOsm), the CD site is the most sensitive and vulnerable portion that first swells and from which causes the subsequent sperm tail deformation. And even in wild-type mice, there are nearly 20% of sperm undergoing this kind of tail deformation during postcopulation. In this regard, what is the physiological function of the CD? Why sperm keep it as a weakness point during transit from the male to female reproductive tract? As optimal fertilization happens in a physiological hypotonic environment (300-340 mOsm) compared with the male reproductive tract [41] and the CD is a transient cellular structure with its function in fertilization still debatable [38], our data would support a novel hypothesis that the temporary presence of the CD in postcopulatory sperm might serve as a guardian in optimizing male fertility, by at one hand sensing external hypotonic changes to convey subsequent signals that stimulate sperm motility, while on the other hand filtering out (by inducing tail deformation) unqualified sperm that could not resist the natural hypotonic stress, thus guaranteeing that fertilization happens in optimal osmotic environment with optimal sperm. Notably, recent evidence has shown that sperm tail coiling was commonly found in ejaculates of infertile patients, suggesting defects in cell volume regulation [25]. As AQP3 is also intensely localized in human sperm, the information obtained from present study in mice should provide valuable insights to further understand the causes of infertility/subfertility in relevant clinical patients.

Materials and Methods

Mice and breeding assay

AQP3 knockout mice were generated as described previously [24]. All the CD1 female mice used in this study were purchased from Vital River Lab Animal Technology Co., Ltd (Beijing, China). Males of different genotypes (8-9 weeks) were used for breeding assay. Each male mouse was caged with a wild-type CD1 female (7-8 weeks) and vaginal plug was checked every morning. Once a vaginal plug was identified (day 1 postcoitus), the

male was allowed to rest for 2 days, after which another female was placed in the cage for another round of mating. The plugged female was separated and single caged, and the pregnancy results were recorded. If a female generated no pups until day 22 postcoitus, it was deemed as not pregnant after sacrificed for confirmation. Each male underwent four cycles of the above breeding assay.

RNA extraction and RT-PCR

RNA extraction, reverse transcription and PCR were performed as previously described [42]. The primers used in this study were provided in Supplementary information, Table S1.

Immunofluorescence on tissue sections and isolated sperm

Frozen sections (10 μm) were fixed in 4% paraformaldehyde (PFA) for 10 min at room temperature. Mouse sperms (from cauda epididymis) and human sperms (ejaculated sperm donated by volunteers with proven fertility) were washed in PBS, fixed in 4% PFA for 30 min at room temperature and air dried onto poly-L-lysine-treated slides. AQP3 polyclonal antibody (AB3276, Millipore) was used at 1:500 for mouse and 1:200 for human. For immunogen-competing assay, the competing peptide was mixed with antibody at 1:1 concentration before incubation.

Scanning, transmission and immunogold electronic microscopy

The scanning and transmission electron microscopy followed standard protocols performed at the Laboratory of Electron Microscopy, Peking University Health Science Center. For the immunogold electron microscopy, the sperm was fixed in 4% PFA, infused in 10% gelatin, dehydrated in sucrose and then frozen in liquid nitrogen. Cryosections (50 nm) were prepared (Leica ULTRACUT UCT/Leica EMFCS) and incubated at room temperature with 0.1% cold water fish skin gelatin (CWFS gelatin, AURION) and 5% BSA for 30 min, then incubated with AQP3 polyclonal antibody (AB3276, Millipore; 1:50) overnight. After extensive washing in PBS, cryosections were then incubated with colloidal gold-conjugated secondary antibody (15 nm gold particle, Goat-anti-Rabbit, AURION). Sections were then stained with uranyl acetate and methylcellulose, and observed by transmission electronic microscopy.

Sperm analysis in utero and in cauda epididymis

Male and female mice were caged together to induce copulation, and vaginal plug was checked every hour. After finding of the vaginal plug, the female was separated and sacrificed 2 or 8 h later; the uterine content was recovered and smeared onto a glass slide for sperm observation under microscope. To check the *in situ* status of sperm morphology before ejaculation, the cauda epididymis and vas deferens were undergone immediate immersive fixation in 5% glutaraldehyde [43]. After 1 h fixation, sperms were punctured/squeezed from the cauda epididymis and vas deferens for morphological examination under light microscope.

Osmolarity measurement

Measurement of osmolarity in uterine content (2 and 8 h after copulation) and cauda epididymis fluid (coupled with vas deferens fluid) was performed on a Vapor pressure osmometer (VAPRO model 5520, Wescor Inc., Utah, USA) as described previously [26].

Sperm osmotic gradient challenge assay

Sperm analysis in different osmotic gradient was performed by directly releasing cauda epididymis sperm into NaCl solution or HTF media (Millipore) with different osmolarities (440, 300, 220 and 150 mOsm). After 15 min incubation at 37 ºC, sperm morphology was analyzed under phase contrast microscope.

Sperm volume analyses

The sperm volume changes were monitored, as reflected in the changes of FSC pattern using a Flow Cytometer (BD FACSAria) as described previously [27]. In brief, the cauda epididymis was punctuated by a needle and sperms were released directly into NaCl solution with different osmolarity at 37 ºC. After 15 min incubation, a total of 10 000 cells was analyzed and recorded for each sample. Data was then exported by Flowjo5.7.2 software for image presentation and statistics.

Time-lapse microscopic analyses

Cauda epididymal sperms were released and exposed to NaCl solution (300 mOsm, 37 ºC), within 3 min after releasing, 10 μl supernatant was pipetted onto a glass slide held by a Slide Warmer at 37 ºC (#720230, Hamilton Thorne Research, Beverly, MA). The time-lapse image of sperm was captured and recorded by NIS-BR software under NIKON microscope (ECLIPSE 80i).

Sperm motility analyses

For mouse sperm motility analysis, a CASA system (Version.12 CEROS, Hamilton Thorne Research) was used with the following settings: for cell detection: minimal contrast, 50; minimal cell size, 4 pixels; and 60 frames were acquired at a frame rate of 60 Hz. At least 200 tracks were measured for each specimen at 37 ºC with a Slide Warmer (#720230, Hamilton Thorne Research).

In vitro and in vivo fertilization analyses

In vitro fertilization was performed under standard protocols as previously described [44]. For *in vivo* fertilization rate, wild-type CD1 females were mated with wild-type or *Aqp3*$^{-/-}$ males, the fertilization rate was examined by counting two-cell rate flushed from the oviduct at 15:00-16:00 of day 2 postcoitus (the morning finding of vaginal plug was designated as day 1 postcoitus).

In vivo examination of sperm entry into the egg-cumulus complex

In vivo examination of sperm entry into the egg-cumulus complex after time-defined copulation was performed according to protocols previously described [28]. In brief, males were caged with wild-type CD1 females for a 3 h period (9-11 h after hCG), vaginal plugs were checked every hour, oviducts were isolated 2.5 h after copulation and the numbers of sperm within the egg/cumulus complex were examined.

In vitro sperm migration assay

In vitro sperm migration assay was modified based on previous report [45]. Transwell plate with different pores in the polycarbonate membrane (3 μm, cat#3415; 5 μm, cat#3421 or 8 μm, cat#3422; Corning, Transwell®) was used for sperm migration assay. Cauda epididymal sperm were initially placed in the lower chamber, after 30 min incubation, upper and lower chamber sperm densities were counted by Flow Cytometer (BD FACSAria).

Statistical analysis

Statistical analyses were performed with SPSS 11.5. The significance of pregnancy rate between *Aqp3*$^{-/-}$ and wild-type or heterozygous males was tested by rank-sum test. Other statistical analyses between *Aqp3*$^{-/-}$ and wild-type were done using unpaired two-tailed *t*-test.

Acknowledgments

We are grateful to Dr Alan S Verkman (University of California, San Francisco, USA) for providing us with AQP3 KO mice and his critical comments on the manuscript. We thank Drs Haibin Wang (Institute of Zoology, Chinese Academy of Sciences), Aaron JW Hsueh (Stanford University, USA) and X Johné Liu (Ottawa Hospital Research Institute, Canada) for their thoughtful discussions throughout the work, and Xin Chang (Peking University) for technical support in immunogold assay. This research was supported by the National Basic Research Program of China 2006CB504006, 2011CB710905 (to ED), 2007CB947401, 2011CB944401 (to YC) and 2006CB504002 (to QS), and Sciences Knowledge Innovation Program of Chinese Academy of Sciences KSCX2-YW-R-080 (to ED).

References

1 Morisawa M, Suzuki K. Osmolality and potassium ion: their roles in initiation of sperm motility in teleosts. *Science* 1980; **210**:1145-1147.
2 Cosson J, Groison AL, Suquet M, *et al*. Marine fish spermatozoa: racing ephemeral swimmers. *Reproduction* 2008; **136**:277-294.
3 Johnson AL, Howards SS. Hyperosmolality in intraluminal fluids from hamster testis and epididymis: a micropuncture study. *Science* 1977; **195**:492-493.
4 Cooper TG, Yeung CH. Acquisition of volume regulatory response of sperm upon maturation in the epididymis and the role of the cytoplasmic droplet. *Microsc Res Tech* 2003; **61**:28-38.
5 Rossato M, Di Virgilio F, Foresta C. Involvement of osmosensitive calcium influx in human sperm activation. *Mol Hum Reprod* 1996; **2**:903-909.
6 Zanetti N, Mayorga LS. Acrosomal swelling and membrane docking are required for hybrid vesicle formation during the human sperm acrosome reaction. *Biol Reprod* 2009; **81**:396-405.
7 Willoughby CE, Mazur P, Peter AT, Critser JK. Osmotic tolerance limits and properties of murine spermatozoa. *Biol Reprod* 1996; **55**:715-727.
8. Drevius LO, Eriksson H. Osmotic swelling of mammalian spermatozoa. *Exp Cell Res* 1966; **42**:136-156.
9 Drevius LO. Spiralization in tails of mammalian spermatozoa in hypotonic media. *Nature* 1963; **197**:1123-1124.
10 Yeung CH, Barfield JP, Cooper TG. Physiological volume regulation by spermatozoa. *Mol Cell Endocrinol* 2006; **250**:98-105.
11 Curry MR, Redding BJ, Watson PF. Determination of water permeability coefficient and its activation energy for rabbit spermatozoa. *Cryobiology* 1995; **32**:175-181.
12 Noiles EE, Mazur P, Watson PF, Kleinhans FW, Critser JK. Determination of water permeability coefficient for human spermatozoa and its activation energy. *Biol Reprod* 1993; **48**:99-109.
13 Drevius LO. Permeability coefficients of bull spermatozoa for water and polyhydric alcohols. *Exp Cell Res* 1971; **69**:212-216.
14 Callies C, Cooper TG, Yeung CH. Channels for water efflux and influx involved in volume regulation of murine spermatozoa. *Reproduction* 2008; **136**:401-410.
15 Yeung CH, Barfield JP, Cooper TG. The role of anion channels and Ca2+ in addition to K+ channels in the physiological volume regulation of murine spermatozoa. *Mol Reprod Dev* 2005; **71**:368-379.
16 Petrunkina AM, Harrison RA, Ekhlasi-Hundrieser M, Topfer-Petersen E. Role of volume-stimulated osmolyte and anion channels in volume regulation by mammalian sperm. *Mol Hum Reprod* 2004; **10**:815-823.
17 King LS, Kozono D, Agre P. From structure to disease: the evolving tale of aquaporin biology. *Nat Rev Mol Cell Biol* 2004; **5**:687-698.
18 Curry MR, Millar JD, Watson PF. The presence of water channel proteins in ram and human sperm membranes. *J Reprod Fertil* 1995; **104**:297-303.
19. Ishibashi K, Kuwahara M, Kageyama Y, *et al*. Cloning and functional expression of a second new aquaporin abundantly expressed in testis. *Biochem Biophys Res Commun* 1997; **237**:714-718.
20 Ishibashi K, Kuwahara M, Gu Y, *et al*. Cloning and functional expression of a new water channel abundantly expressed in the testis permeable to water, glycerol, and urea. *J Biol Chem* 1997; **272**:20782-20786.
21 Yeung CH, Callies C, Rojek A, Nielsen S, Cooper TG. Aquaporin isoforms involved in physiological volume regulation of murine spermatozoa. *Biol Reprod* 2009; **80**:350-357.
22 Sohara E, Ueda O, Tachibe T, *et al*. Morphologic and functional analysis of sperm and testes in Aquaporin 7 knockout mice. *Fertil Steril* 2007; **87**:671-676.
23 Yang B, Song Y, Zhao D, Verkman AS. Phenotype analysis of aquaporin-8 null mice. *Am J Physiol Cell Physiol* 2005; **288**:C1161-C1170.
24 Ma T, Song Y, Yang B, *et al*. Nephrogenic diabetes insipidus in mice lacking aquaporin-3 water channels. *Proc Natl Acad Sci USA* 2000; **97**:4386-4391.
25 Yeung CH, Callies C, Tuttelmann F, Kliesch S, Cooper TG. Aquaporins in the human testis and spermatozoa–identification, involvement in sperm volume regulation and clinical relevance. *Int J Androl* 2009; **33**:629-641.
26 Yeung CH, Wagenfeld A, Nieschlag E, Cooper TG. The cause of infertility of male c-ros tyrosine kinase receptor knockout mice. *Biol Reprod* 2000; **63**:612-618.
27 Yeung CH, Anapolski M, Cooper TG. Measurement of volume changes in mouse spermatozoa using an electronic sizing analyzer and a flow cytometer: validation and application to an infertile mouse model. *J Androl* 2002; **23**:522-528.
28 Sutton KA, Jungnickel MK, Florman HM. A polycystin-1 controls postcopulatory reproductive selection in mice. *Proc Natl Acad Sci USA* 2008; **105**:8661-8666.
29 Hoffmann EK, Lambert IH, Pedersen SF. Physiology of cell

volume regulation in vertebrates. *Physiol Rev* 2009; **89**:193-277.
30 Hill AE, Shachar-Hill B, Shachar-Hill Y. What are aquaporins for? *J Membr Biol* 2004; **197**:1-32.
31 Kuang K, Yiming M, Wen Q, *et al*. Fluid transport across cultured layers of corneal endothelium from aquaporin-1 null mice. *Exp Eye Res* 2004; **78**:791-798.
32 Ford P, Rivarola V, Chara O, *et al*. Volume regulation in cortical collecting duct cells: role of AQP2. *Biol Cell* 2005; **97**:687-697.
33 Liu X, Bandyopadhyay BC, Nakamoto T, *et al*. A role for AQP5 in activation of TRPV4 by hypotonicity: concerted involvement of AQP5 and TRPV4 in regulation of cell volume recovery. *J Biol Chem* 2006; **281**:15485-15495.
34 Kida H, Miyoshi T, Manabe K, *et al*. Roles of aquaporin-3 water channels in volume-regulatory water flow in a human epithelial cell line. *J Membr Biol* 2005; **208**:55-64.
35 Gadsby DC. Ion channels versus ion pumps: the principal difference, in principle. *Nat Rev Mol Cell Biol* 2009; **10**:344-352.
36 Waight AB, Love J, Wang DN. Structure and mechanism of a pentameric formate channel. *Nat Struct Mol Biol* 2010; **17**:31-37.
37 Wang Y, Huang Y, Wang J, *et al*. Structure of the formate transporter FocA reveals a pentameric aquaporin-like channel. *Nature* 2009; **462**:467-472.
38 Cooper TG. Cytoplasmic droplets: the good, the bad or just confusing? *Hum Reprod* 2005; **20**:9-11.
39 Lishko PV, Botchkina IL, Fedorenko A, Kirichok Y. Acid extrusion from human spermatozoa is mediated by flagellar voltage-gated proton channel. *Cell* 2010; **140**:327-337.
40 Kirichok Y, Navarro B, Clapham DE. Whole-cell patch-clamp measurements of spermatozoa reveal an alkaline-activated Ca2+ channel. *Nature* 2006; **439**:737-740.
41 Miyamoto H, Chang MC. Effect of osmolality on fertilization of mouse and golden hamster eggs *in vitro*. *J Reprod Fertil* 1973; **33**:481-487.
42 Kuang H, Chen Q, Fan X, *et al*. CXCL14 inhibits trophoblast outgrowth via a paracrine/autocrine manner during early pregnancy in mice. *J Cell Physiol* 2009; **221**:448-457.
43 Sipila P, Cooper TG, Yeung CH, *et al*. Epididymal dysfunction initiated by the expression of simian virus 40 T-antigen leads to angulated sperm flagella and infertility in transgenic mice. *Mol Endocrinol* 2002; **16**:2603-2617.
44 Xu WM, Shi QX, Chen WY, *et al*. Cystic fibrosis transmembrane conductance regulator is vital to sperm fertilizing capacity and male fertility. *Proc Natl Acad Sci USA* 2007; **104**:9816-9821.
45 Baibakov B, Gauthier L, Talbot P, Rankin TL, Dean J. Sperm binding to the zona pellucida is not sufficient to induce acrosome exocytosis. *Development* 2007; **134**:933-943.

(**Supplementary information** is linked to the online version of the paper on the *Cell Research* website.)

Supplementary information

Manuscript title: “Aquaporin3 is a sperm water channel essential for post-copulatory sperm osmo-adaptation and migration”

Author list: Qi Chen, Hongying Peng, Li Lei, Ying Zhang, Haibin Kuang, Yujing Cao, Qi-xian Shi, Tonghui Ma, Enkui Duan

Supplementary Figures and Legends

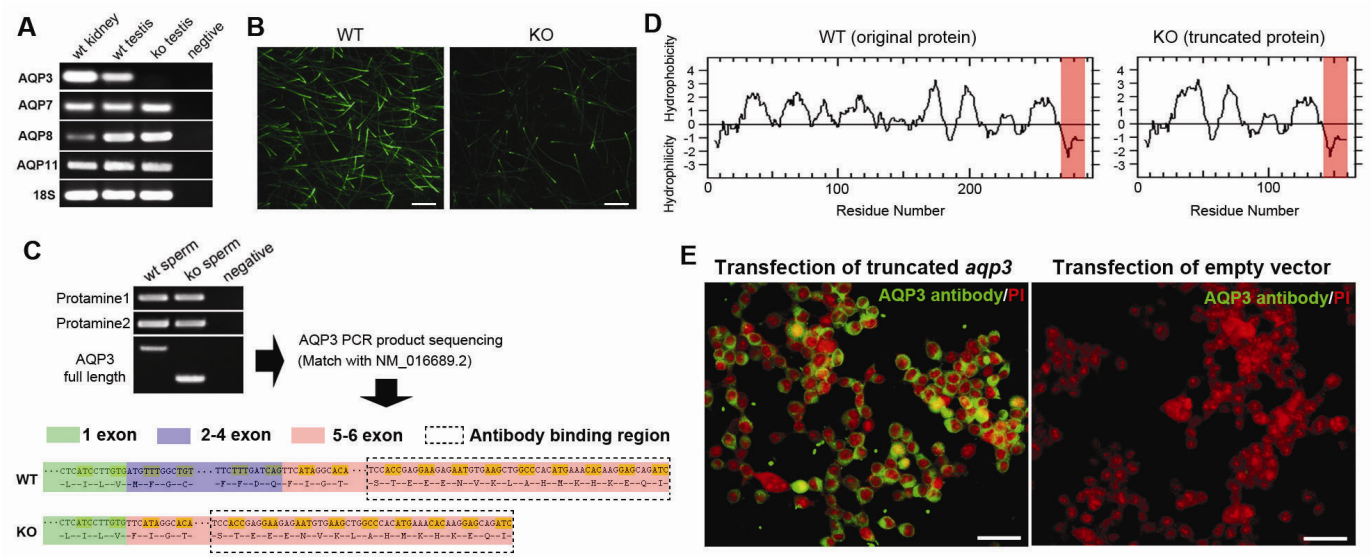

Supplementary Figures S1. AQP3 expression in testis and sperm. **A.** Semiquantitative RT-PCR detection of AQP3, 7, 8, 11 in testis. AQP3 primers designed within exon 3. **B**. Immunofluorescence detection of AQP3 in sperm. Scale bars represent 20 μm. It should be noted that sperm from *Aqp3*$^{-/-}$ mice also showed positive staining, although the intensity is lower. This is because the *Aqp3*$^{-/-}$ sperm could express a truncated aqp3 transcript as shown in panel (**C,D,E**). **C.** Full length aqp3 PCR detection showed that sperms from both wildtype and *Aqp3*$^{-/-}$ mice express aqp3 mRNA, the *Aqp3*$^{-/-}$ sperm express a truncated aqp3 transcript lacking exons 2-4, retaining a full sequence of exon1 linking with exons 5-6, which could be translated into a nonfunctional peptide containing the antibody detection region (c-terminal). Protamine1 and 2 were used as an internal control for sperm mRNA. **D.** Kyte-Doolittle analyses showed hydrophobic scores of original and truncated AQP3 protein, suggesting the truncated AQP3 protein is highly hydrophobic with three predicted transmembrane domain, leaving the hydrophilic c-terminal detectable by the antibody. The red shaded region demonstrate antibody detection region. **E**. The KO truncated *aqp3* was obtained and subcloned into the vector pcDNA4/TO/MycHis B (invitrogen), then transfected into 293T cells using FuGENE (Roche) following manufacture’s instructions. After Zeocin selection, cells were processed for AQP3 immunofluorence assay and showed cytoplasmic/membrane localization. These results explained the observed positive AQP3 staining in *Aqp3*$^{-/-}$ sperm. scale bar:50μm. For each data presented, results were repeated in 2-3 independent mice.

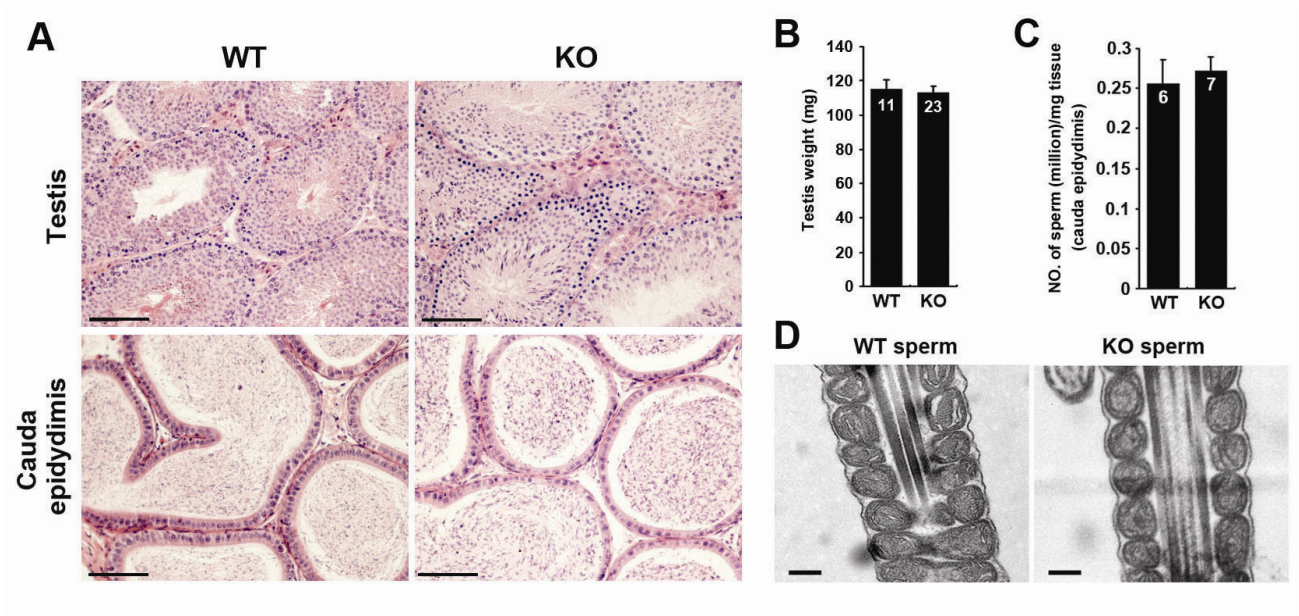

Supplementary Figures S2. Morphological and histological examination of testis, epididymis and sperm count between wildtype and *Aqp3*$^{-/-}$ mice. **A.** Paraformaldehyde fixed, hematoxylin/eosin-stained sections of testis and epididymis. Scale represents 20 μm. **B,C.** Testicular weight (**B**) (after 24 hours fixation in Paraformaldehyde) and sperm count (**C**) is comparable between wildtype and *Aqp3*$^{-/-}$ male ($P > 0.05$, Student's t test). Numbers within the bars indicate number of mice used for each assay. Error bars represent s.e.m. **D.** Ultrastructural analyses of wildtype and *Aqp3*$^{-/-}$ sperm reveals comparable internal tail structure. Scale bars represent 0.2 μm.

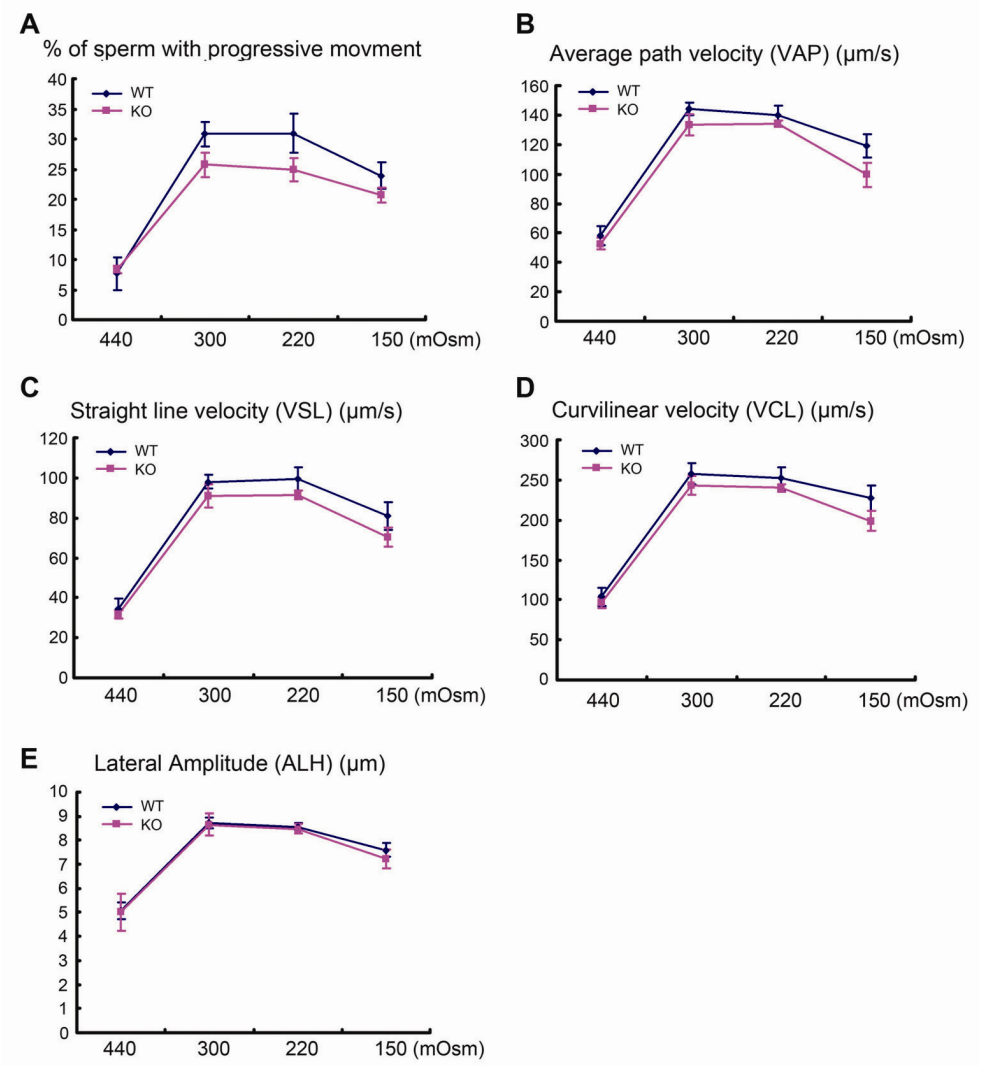

Supplementary Figures S3. Physiological hypotonic stress stimulates sperm motility "start up" in both wildtype and *Aqp3*$^{-/-}$ sperm. Cauda epididymal sperm from both genotypes were directly released into NaCl solution with different osmolarity. The motion parameters were analyzed and recorded by a CASA analysis system. All data represented are obtained 10 min after releasing into solution. **a.** Percentage of sperm with progressive movement (VAP>50um/s, STR (VSL/VAP)>80%). **b.** Average path velocity (VAP). **c.** Straight line velocity (VSL). **d.** Curvilinear velocity (VCL). **e.** Amplitude of lateral head displacement (ALH). For each presented motility parameter, there is a significant change between 440 and 300 mOsm ($P < 0.00001$, *t*-test). No statistical significance was found between wildtype and *Aqp3*$^{-/-}$ group ($P > 0.05$, *t*-test), although some parameters shows slightly decrease in *Aqp3*$^{-/-}$ group. 5-9 mice were used for each osmolarity. All error bars represent s.e.m.

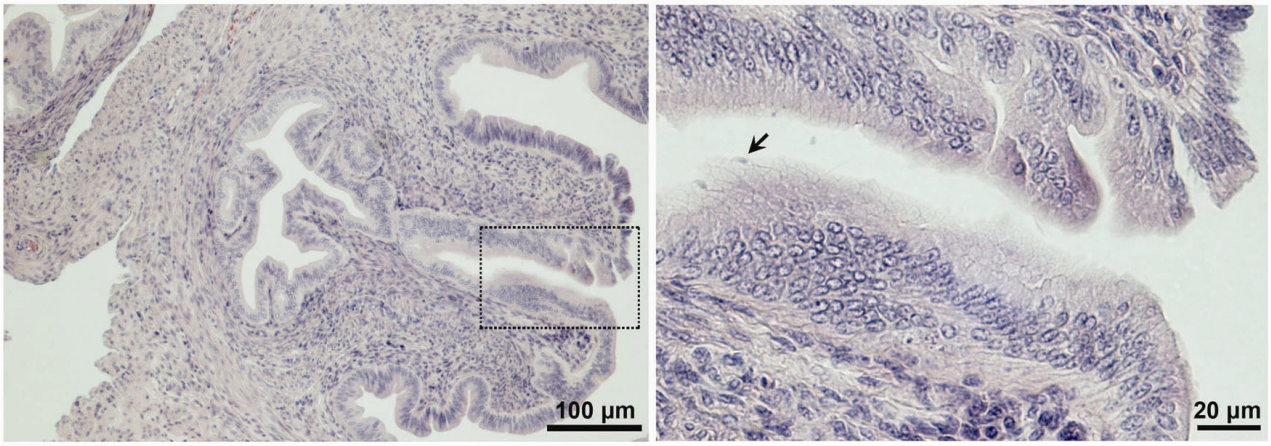

Supplementary Figures S4. Tissue sections showing example of sperms transportation through uterine-oviduct junction (2 h after copulation) .Sperms were indicated by arrows.

Supplementary Movie legends

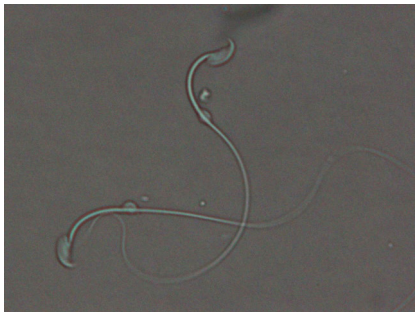

Supplementary Movie S1

Cauda epididymal sperm from wildtype mouse released into 300 mOsm NaCl solution, showing mild swelling at cytoplasmic droplet.

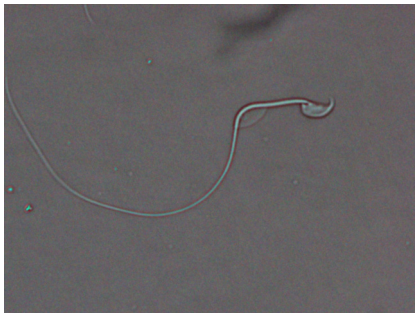

Supplementary Movie S2

Cauda epididymal sperm from *Aqp3*$^{-/-}$ mouse released into 300 mOsm NaCl solution, showing progressive swelling at cytoplasmic droplet that forced sperm tail deformation.

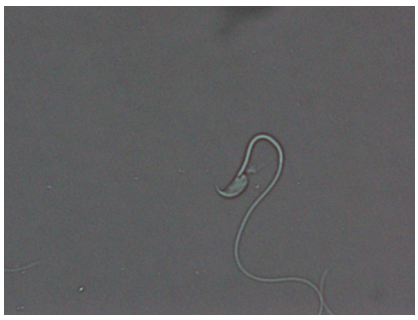

Supplementary Movie S3

Cauda epididymal sperm from *Aqp3*$^{-/-}$ mouse released into 300 mOsm NaCl solution, showing progressive swelling at cytoplasmic droplet that forced sperm tail deformation and membrane rupture.

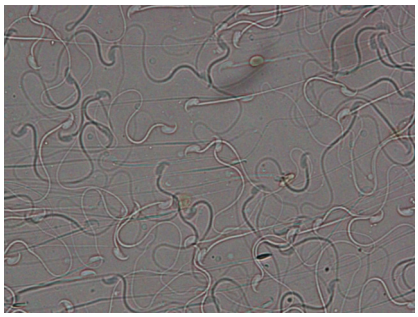

Supplementary Movie S4

Wildtype sperm recovered from uterus 2h after copulation (wildtype male mate with wildtype female). Most sperms showed normal motility without tail deformation.

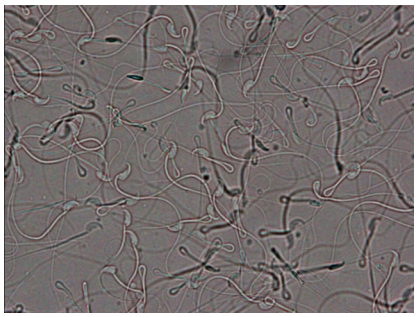

Supplementary Movie S5

Aqp3$^{-/-}$ sperm recovered from uterus 2h after copulation (*Aqp3*$^{-/-}$ male mate with wildtype female). A large portion of sperm showed hairpin-like tail deformation with low/no motility, while sperms without tail deformation kept normal motility.

Supplementary Table S1. Primers used for RT-PCR

Transcript	Forward primer(5'-3')	Reverse primer(5'-3')
AQP3	GCCCATCTATGCACTGGCA	CGAAAAGCTCATTGTTGGCAA
AQP3 full length	AGCTACTTTGCACTCGTACG	GATCTGCTCCTTGTGTTTCATG
AQP7	TCGTGACTGGGATGCTGC	ACGGGATGGGTTGATTGC
AQP8	CAGCCTTTGCCATCGTCCAGG	CCTAATGAGCAGTCCTACAAAG
AQP11	GCCTTCGTCCTGGAGTTT	TCCTTTCGTCGTAATGGTAC
protamine1	GCTCACAGGTTGGCTGGCTCG	TGGTGTATGAGCGGCGGCGA
Protamine2	GAGCGCGTAGAGGACTATGG	CAGACATCGACATGGAATGG
18S	AATCAGGGTTCGATTCCGGA	CCAAGATCCAACTACGAGCT